Improved electrical characteristics of $Al_xGa_{1-x}N$/GaN High Electron Mobility Transistor by effect of physical and geometrical parameters

A. Douara
Faculty of Science and Technology, Tissemsilt University, Algeria.

A. Rabehi
Laboratoire de Micro-électronique Appliquée,
Université Djillali Liabés de Sidi Bel Abbés, BP 89, 22000, Sidi Bel Abbés, Algeria.
Faculty of Science and Technology, Ziane Achour University of Djelfa, Djelfa, Algeria.

O. Baitiche
Laboratory of Semi-conductors and Functional materials, Ammar Thlidji University of Laghouat, Algeria.

M. Hamdani
Faculty of Science and Technology, Tissemsilt University, Algeria.

Received 26 August 2022; accepted 2 January 2023

This research aims to study the impact of some physical and structural parameters on the I-V characteristics of a high electron mobility transistors (HEMTs) based on $Al_xGa_{1-x}N$/GaN. We investigate the effect of the GaN buffer layer thickness and the impact of other properties of the materials such as aluminum mole fraction and doping concentration, the $Al_{0.2}Ga_{0.8}N$/GaN heterostructures with 400 nm of buffer layer and a layer doped with $n = 4\times10^{18}$ cm^{-3}, for this structure we find the maximum saturation current of 420 mA/mm. The proposed model included GaN buffer layer and Al content were derived from our developed I-V characteristics. The proposed model is in excellent agreement with the simulated I-V characteristics and experimental results.

Keywords: HEMTs; $Al_xGa_{1-x}N$/GaN; buffer layer; GaN.

DOI: https://doi.org/10.31349/RevMexFis.69.041001

1. Introduction

AlGaN/GaN-based high electron mobility transistors have been explored for high frequency, high power switching applications as III-V materials that have high electron saturation velocity ($> 2.5\times10^7$ cm/s, 2.5 times of that of silicon) , high chemical stability and high breakdown field ($>$ 3 MV/cm, 10 times of that of silicon) [1,2].

Due to their superior properties compared to other materials, materials based on III-V semiconductors and its alloys have become the prospect of an efficient microwave power device [3-7]. Frequently, the breakdown of a GaN-based HEMTs is determined by the sub threshold drain current exceeding the standard value of 1 mA/mm [8].

The basic principle of HEMTs is the formation of a heterojunction by two semiconductors at different bandgaps.The concentration of two dimensional electron gas (2DEG) can be controlled by doping the $Al_xGa_{1-x}N$ layer and Al content [9,10]. The performance enhancement of AlGaN/GaN heterostructures can be accomplished with high carrier sheet concentration (10^{13} cm^{-2}) beyond those possible in other III-V material systems by a significant margin [11-15].

The analysis of I-V characteristics of the device performance is a crucial step for the development of a physics based compact model for devices [16]. The I-V characteristics of AlGaN/GaN HEMTs were presented in the model proposed in Refs. [16,17] based on the device physics. However, the effect of δ -doping the AlGaN barrier layer and the GaN buffer layer thickness were not taken into consideration.

In this paper, the current - voltage study has been simulated using 2D Silvaco Atlas device simulation software. The derivation of the core current model is presented in Sec. 2. Our improved devices of the AlGaN/GaN HEMTs were examined to see how certain parameters influenced the I-V characteristics in Sec. 3. To assess and put into practice the proposed model in [16,17], the transfer and output characteristics results and experimental data [18] are compared.

2. Model development for drain current

2.1. Core drain current

The drain to source current model is mainly derived from the charge control model reported in Ref. [19]:

$$I_{DS} = \frac{q\mu W}{L}\left[\frac{qd}{2\varepsilon}\left(n_D^2 - n_S^2\right) + \frac{2}{5}\gamma_0\left(n_D^{5/3} - n_S^{5/3}\right)\right] + V_{th}\left(n_S - n_D\right). \quad (1)$$

The sheet carrier density of 2DEG is given by:

$$n_s = DV_{th}\ln\left(\exp\left[\frac{E_f - E_0}{V_{th}}\right] + 1\right), \quad (2)$$

TABLE I. List of symbols.

Symbol	Description
q	Elementary charge
μ	Carrier mobility
W	Channel width
L	Channel length
d_c	GaN channel layer thickness
d_b	AlGaN barrier layer thickness
ε	Permittivity of AlGaN barrier layer
n_s	2DEG density
n_D	Charge carrier concentration at drain
γ_0	Constant estimated experiment [21]
V_{th}	Threshold voltage
E_f	Position Fermi level
E_0	Energy of the first subband
V_{g0}	Applied gate voltage
V_{OFF}	Cut-off /threshold voltage
$\phi_{\text{eff}}(x)$	Schottky barrier height
$E_g^{\text{Al}_x\text{Ga}_{1-x}\text{N}}$	The energy band gap of $Al_xGa_{1-x}N$ layer
E_g^{GaN}	The energy band gap of GaN layer
D	The conduction band density of state

where n_s and n_D can be calculated iteratively from Eq. (3) (reported by [16]):

$$V_{g0} - V = \frac{qdn_s}{\varepsilon} + \gamma_0 n_s^{2/3} + V_{th}\ln\left(\frac{n_s}{DV_{th}}\right), \quad (3)$$

where

$$V_{g0} = V_g - V_{\text{OFF}}, \quad (4)$$

where V_{OFF} is the cutoff voltage

$$V_{\text{OFF}} = \phi_{\text{eff}}(x) - 0.7\left[E_g^{\text{AlxGa1-xN}} - E_g^{\text{GaN}}\right] - \frac{1}{2}\left[\frac{qN_Dd_b^2 - \sigma_{\text{total}}\,d_b}{0.3x + 10.4}\right]. \quad (5)$$

The total induced polarization at the interface is given by [20]:

$$\sigma_{total} = P_{pz} - P_{sp}. \quad (6)$$

Table I illustrates the standard definitions of the symbols used.

3. Device structure

Our simulations of the AlGaN/GaN-based HEMTs transistor were carried out using the structure shown in Fig. 1. This structure is formed by a $Al_xGa_{1-x}N$ barrier layer of 30 nm intentionally δ -doped with an N_D dopant, and 50 nm of GaN channel layer doped with an approximated doping level of 3×10^{17} cm^{-3}, and GaN buffer layer deposited on an Al_2O_3 insulating sapphire substrate. All structures were simulated with a gate length of 2 μm and a source-to-drain spacing of 5 μm. The thickness of the GaN buffer layer is taken as a variable parameter in our calculations. In addition, we employed the 2D Atlas TCAD simulator software for numerical simulation.

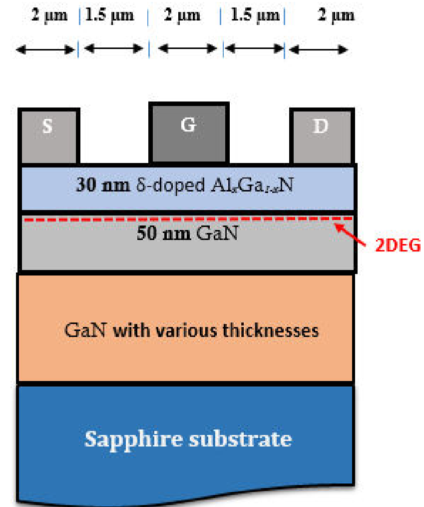

FIGURE 1. Cross sectional $Al_xGa_{1-x}N$/GaN HEMT structure in our study.

4. Results and discussions

4.1. Influence of GaN buffer layer thickness

Figure 2 illustrates the $I_{DS} - V_{DS}$ characteristics calculated of HEMT AlGaN/GaN, we report that the drain current thickness of the GaN layer are inversely proportional. However, the I_{DS} current at $V_{GS} = 0$ is considerably huge as a result of the high conductivity of 400 nm thick GaN layers.

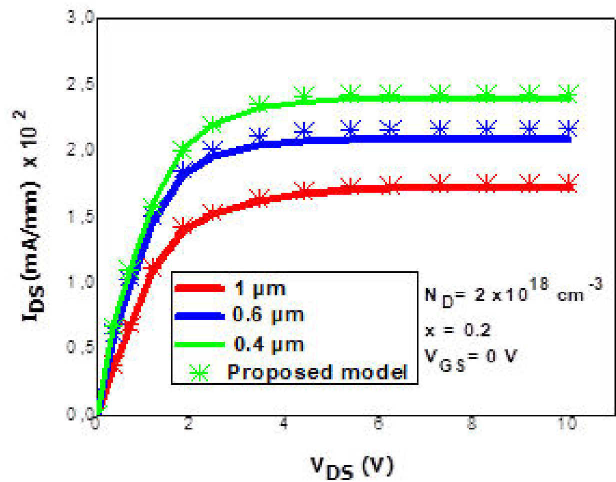

FIGURE 2. Comparison of modeled results (symbols) with Silvaco ATLAS data (solid line) output characteristics of $Al_{0.2}Ga_{0.8}N$/GaN HEMTs for different GaN buffer layer thickness values.

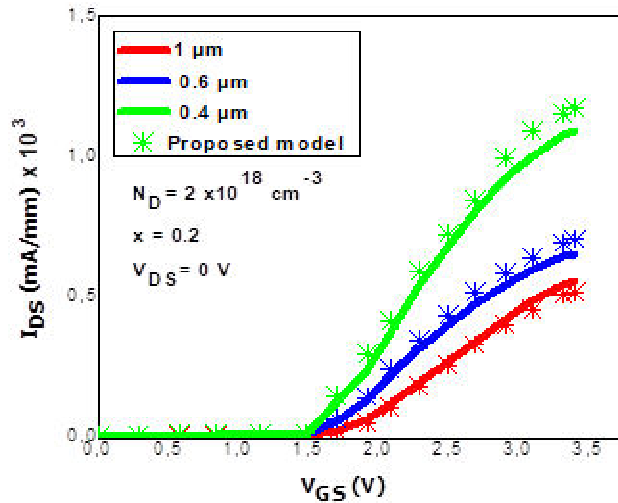

FIGURE 3. Comparison of modeled results (symbols) with Silvaco ATLAS data (solid line) transfer characteristics of $Al_{0.2}Ga_{0.8}N$/GaN HEMTs for different GaN buffer layer thickness values.

Figure 3 illustrates the transfer characteristics of our structure when $V_{DS} = 0$, the curves indicate that we can reach a high electron density, by firstly reducing impurity scattering and improving the transconductance of our devices and also by increasing the electron mobility in the channel.

4.2. Influence of δ-doping the AlGaN barrier layer

In this section we investigated the impact of varying the concentration of donors $N_D(\delta)$ within the $Al_{0.2}Ga_{0.8}N$ barrier layer and take 400 nm for GaN buffer layer. The results are summarized in the Fig. 4, where the output characteristics shows that the intentional δ- doping barrier layer is necessary to obtain high transconductance. In addition, we can clearly

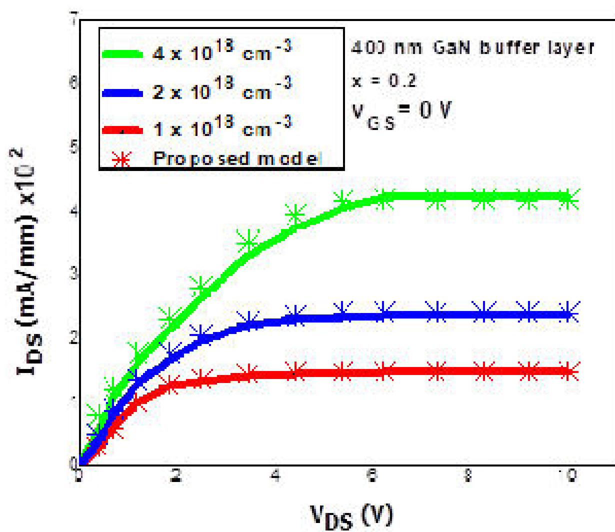

FIGURE 4. Comparison of modeled results (symbols) with Silvaco ATLAS data (solid line) output characteristics of $Al_{0.2}Ga_{0.8}N$/GaN HEMTs for the different values of $N_D(\delta)$.

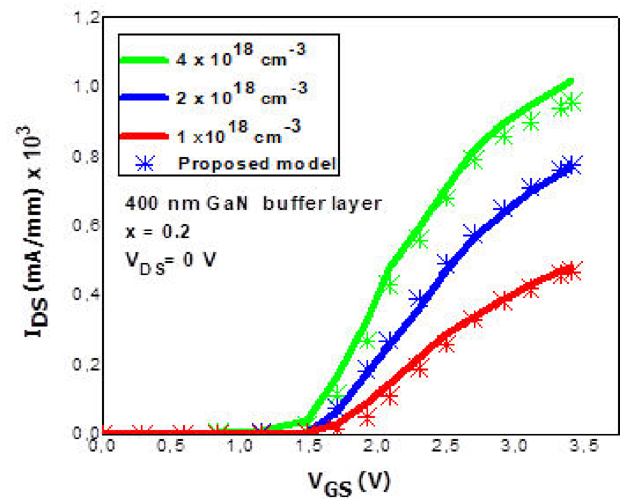

FIGURE 5. Comparison of modeled results (symbols) with Silvaco ATLAS data (solid line) transfer characteristics of $Al_{0.2}Ga_{0.8}N$/GaN HEMTs for the different $N_D(\delta)$ values.

notice in Fig. 4 the strong influence of the dopant $N_D(\delta)$. It is observed here that the source current increases with the increase in δ -doping concentration. $I_{Dmax} = 420$ mA/mm for $N_D(\delta) = 4 \times 10^{18}$ cm^{-3}. The calculation $I_{DS} - V_{GS}$ characteristics reveals that the intentional doping of AlGaN layer is important for obtaining high transconductance.The component exhibits the largest drain saturation current because the barrier layer has the highest doping concentration, as seen in Fig. 5.

4.3. Influence of the molar fraction

Figure 6 shows illustrates the output characteristics of $Al_xGa_{1-x}N$/GaN HEMT For different mole fraction values in the $Al_xGa_{1-x}N$ barrier layer. Our study reports that with a mole fraction of $x = 20\%$, our device achieves the largest source saturation current. $I_{Dssat} = 420$ mA/mm as com-

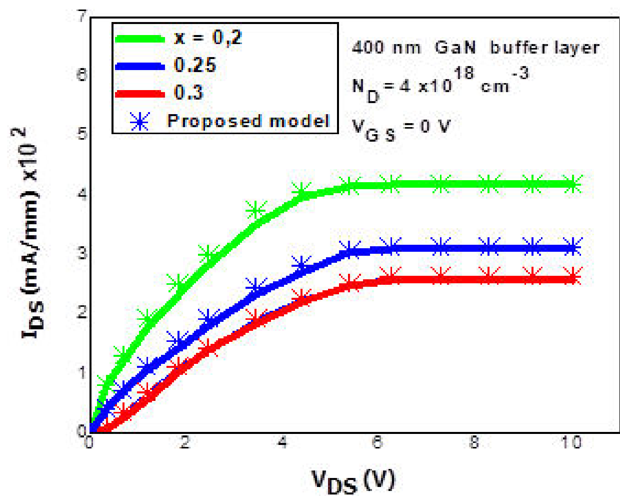

FIGURE 6. Comparison of modeled results (symbols) with Silvaco ATLAS data (solid line) of output characteristics of $Al_xGa_{1-x}N$/GaN HEMTs for different Al content.

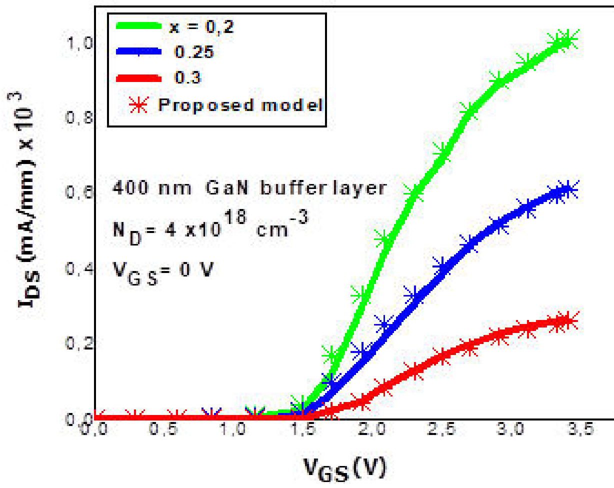

FIGURE 7. Comparison of modeled results (symbols) with Silvaco ATLAS data (solid line) transfer characteristics of $Al_xGa_{1-x}N$/GaN HEMTs for different Al content.

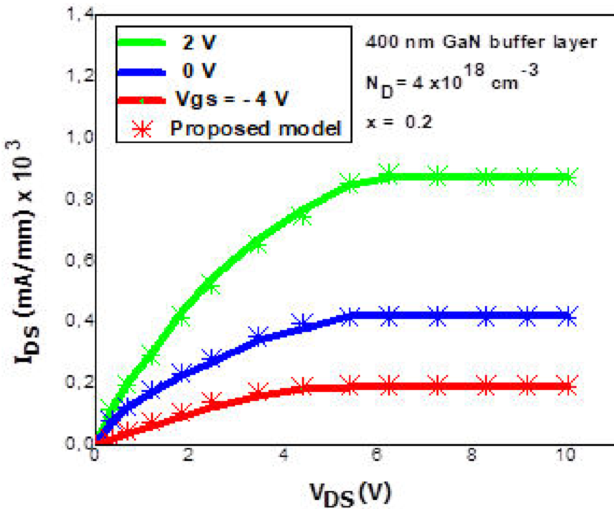

FIGURE 8. Comparison of modeled results (symbols) with Silvaco ATLAS data (solid line) output characteristics of $Al_{0.2}Ga_{0.8}N$/GaN HEMTs for different gate voltage values.

pared to result available with mole fractions of $x = 30\%$ and $x = 25\%$. The $I_{DS} - V_{GS}$ characteristics are shown in Fig. 7, where the HEMT device exhibits a low threshold voltage for $x = 20\%$, the results show that an improvement in the transconductance and the performance of the normally HEMT components can be accomplished by changing the aluminum mole fraction in the $Al_xGa_{1-x}N$ barrier layer.

4.4. Simulation at different voltages

The characteristics of current and voltage are shown in Fig. 8. When the gate-to-source voltage changed from - 4 to + 2 V, a distinguishable field-effect was observed calculated using this device. However the effect of gate leakage can be included in the simulations, The results of $I_{DS} - V_{DS}$ characteristics are plotted, we can observe a high drain current when the gate voltage is lower. It demonstrates strong agreement

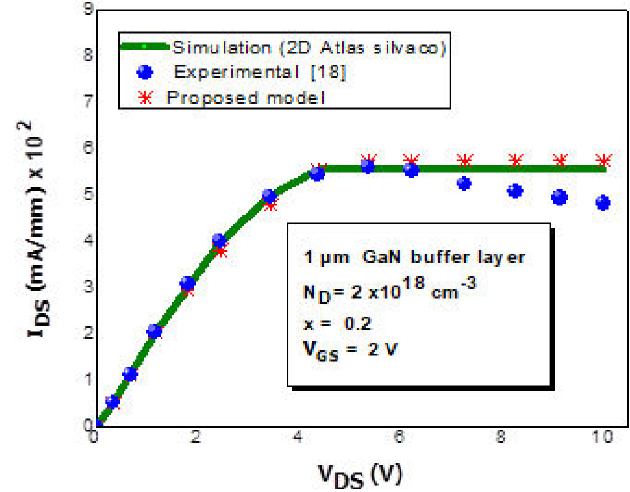

FIGURE 9. Comparison of modeled results (symbols) with Silvaco ATLAS data and experimental [18] of output characteristics of $Al_{0.2}Ga_{0.8}N$/GaN HEMTs.

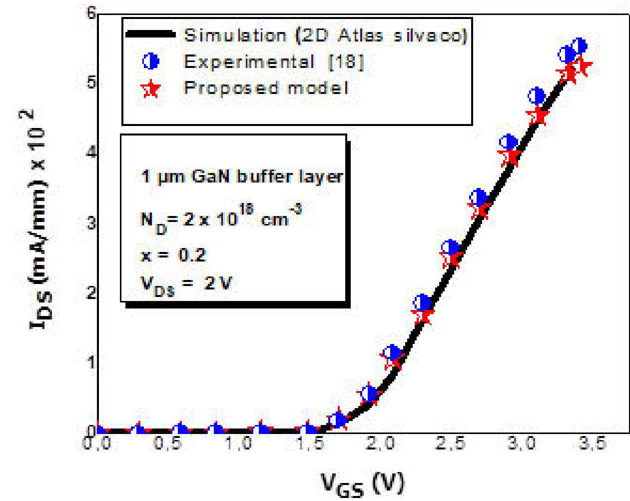

FIGURE 10. Comparison of modeled results (symbols) with Silvaco ATLAS data and experimental [18] of Transfer characteristics of $Al_{0.2}Ga_{0.8}N$/GaN HEMTs.

with the normally-off HEMT devices, according to the curves, we find ($I_{Ds\,\max} = 900$ mA/mm at $V_{DS} = 2$ V).

Our reported data can obviously find a strong agreement with experimental data reported by khan *et al* [18] as illustrated in both Fig. 9 and 10. In Fig. 9, the effects of self heating are not considered in the simulated and the charge transport model of $I_{DS} - V_{DS}$ characteristics, when the lattice temperature increases due to the self-heating effect, the current is remarkably downshifted, and a significant decline in device performance occurs. We can also report the positive correlation between the maximum lattice temperature and power according to simulation results, this effect of self-heating is reported previously in Ref. [22].

5. Conclusion

In our simulation results, we investigated the I-V characteristics of AlGaN/GaN-based HEMTs by Atlas TCAD simulator. The influence of the GaN buffer layer thickness on the electrical characteristics of the AlGaN/GaN heterostructure is considered, other influence parameters are also taken into consideration. The enhancement of drain-source current is due to Al molar fraction and donor concentration within AlGaN barrier layer, in this layer the donor concentration is a more decisive factor than the other parameters that influences the channel's current increase. Additionally, we find that for $V_{GS} = 2$ V, a device with a 400 nm buffer layer, $N_D(\delta) = 4 \times 10^{18}$ cm^{-3}, and a 20%. Al concentration in the barrier layer are the perfect possible parameters choices for our study that exhibits drain source saturation current values.

Among the simulated HEMT structures, the transfer characteristics in this structure exhibit the lowest threshold voltage value and the highest maximum transconductance. The results of proposed models for our device I-V characteristics for different several parameters illustrate a superb agreement with 2D Atlas TCAD data.

1. H.-P. Lee *et al.*, Investigation of AlGaN/GaN high electron mobility transistor structures on 200-mm silicon (111) substrates employing different buffer layer configurations, *Scientific reports* **6** (2016) 1, https://doi.org/10.1038/srep37588.
2. A. Douara *et al.*, Optimization of two-dimensional electron gas characteristics of AlGaN/GaN high electron mobility transistors, *International Journal of Numerical Modelling: Electronic Networks, Devices and Fields* **32** (2019) e2518, https://doi.org/10.1002/jnm.2518.
3. A. Ziane *et al.*, 2D Modélisation Du Comportement De Nouvelle *Structure de Cellule Solaire* (2016).
4. A. Douara *et al.*, 2-D optimisation current-voltage characteristics in AlGaN/GaN HEMTs with influence of passivation layer, *International Journal of Ambient Energy* **42** (2021) 1363, https://doi.org/10.108/01430750.2019.1608856.
5. A. Rabehi *et al.*, Study of the characteristics current-voltage and capacitance-voltage in nitride GaAs Schottky diode, *The European Physical Journal Applied Physics* **72** (2015) 10102, https://doi.org/10.1051/epjap/2015150140.
6. A. Rabehi *et al.*, Electrical and photoelectrical characteristics of Au/GaN/GaAs Schottky diode, *Optik* **127** (2016) 6412, https://doi.org/10.1016/j.ijleo.2016.04.113.
7. A. Rabehi *et al.*, Simulation and experimental studies of illumination effects on the current transport of nitridated GaAs Schottky diode, *Semiconductors* **52** (2018) 1998, https://doi.org/10.1134/S106378261816025X.
8. E. Bahat-Treidel *et al.*, AlGaN/GaN/AlGaN DH-HEMTs breakdown voltage enhancement using multiple grating field plates (MGFPs), *IEEE Transactions on Electron Devices* **57** (2010) 1208, https://doi.org/10.1109/TED.2010.2045705.
9. A. Mohanbabu *et al.*, Modeling of sheet carrier density and microwave frequency characteristics in Spacer based AlGaN/AlN/GaN HEMT devices, *Solid-State Electronics* **91** (2014) 44, https://doi.org/10.1016/j.sse.2013.09.009.
10. K. Biswas, R. Ghoshhajra, and A. Sarkar, High Electron Mobility Transistor: Physics-Based TCAD Simulation and Performance Analysis, *In HEMT Technology and Applications*, pp. 155-179 (Springer, 2023), https://doi.org/10.1007/978-981-19-2165-0_12.
11. B. Yang *et al.*, Influence of Interface Roughness Scattering on Electron Mobility in GaAs-Al0. 3Ga0. 7 as Two Dimensional Electron Gas (2DEG) Heterostructures, *MRS Online Proceedings Library (OPL)* **355** (1994), https://doi.org/10.1557/PROC-355-545.
12. A. Douara *et al.*, IV Characteristics Model For AlGaN/GaN HEMTs Using Tcad-Silvaco (2015), https://doi.org/10.12816/0010326.
13. H. Helal *et al.*, Comparative study of ionic bombardment and heat treatment on the electrical behavior of Au/GaN/n-GaAs Schottky diodes, *Superlattices and Microstructures* **135** (2019) 106276, https://doi.org/10.1016/j.spmi.2019.106276.
14. A. Rabehi *et al.*, Optimal estimation of Schottky diode parameters using a novel optimization algorithm: Equilibrium optimizer, *Superlattices and Microstructures* **146** (2020) 106665, https://doi.org/10.1016/j.spmi.2020.106665.
15. A. Ziane *et al.*, Frequency Dependent Capacitance and Conductance-Voltage Characteristics of Nitride GaAs Schottky Diode, *Semiconductors* **55** (2021) 51, https://doi.org/10.1134/S1063782621010206.
16. F. M. Yigletu *et al.*, Compact charge-based physical models for current and capacitances in AlGaN/GaN HEMTs, *IEEE Transactions on Electron Devices* **60** (2013) 3746, https://doi.org/10.1109/TED.2013.2283525.
17. A. Douara, N. Kermas, and B. Djellouli, Capacitance Models of AlGaN/GaN High Electron Mobility Transistors, *International Journal of Nuclear and Quantum Engineering* **10** (2016) 420.
18. M. A. Khan *et al.*, AlGaN/GaN metal oxide semiconductor heterostructure field effect transistor, *IEEE Electron Device Letters* **21** (2000) 63, https://doi.org/10.1109/55.821668.
19. S. Khandelwal and T. A. Fjeldly, A physics based compact model of I-V and C-V characteristics in AlGaN/GaN HEMT devices, *Solid-State Electronics* **76** (2012) 60, https://doi.org/10.1016/j.sse.2012.05.054.

20. F. Bernardini and V. Fiorentini, Nonlinear macroscopic polarization in III-V nitride alloys, *Phys. Rev. B.* **64** (2001) 085207, https://doi.org/10.1103/PhysRevB.64.085207.

21. D. Delagebeaudeuf and N. T. Linh, Metal-(n) AlGaAs-GaAs two-dimensional electron gas FET, *IEEE Transactions on Electron Devices* **29** (1982) 955, https://doi.org/10.1109/T-ED.1982.20813.

22. A. Nigam *et al.*, Effect of self-heating on electrical characteristics of AlGaN/GaN HEMT on Si (111) substrate, *AIP Advances* **7** (2017) 085015, https://doi.org/10.1063/1.4990868.